

Metal-Enhanced Fluorescence from Silver Nanowires with High Aspect Ratio on Glass Slides for Biosensing Applications

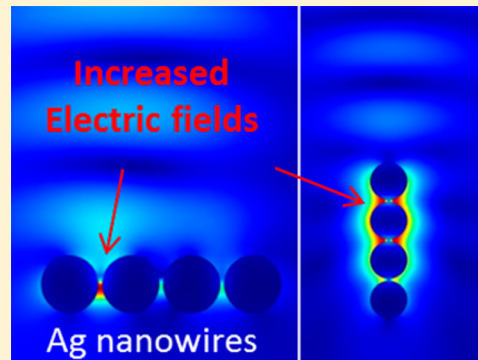
Biebelle Abel,[†] Sahin Coskun,[‡] Muzaffer Mohammed,[†] Richard Williams,[†] Husnu Emrah Unalan,^{*,‡} and Kadir Aslan^{*,†}

[†]Department of Chemistry, Morgan State University, 1700 East Cold Spring Lane, Baltimore, Maryland 21251, United States

[‡]Department of Metallurgical and Materials Engineering, Middle East Technical University, Ankara 06800, Turkey

Supporting Information

ABSTRACT: High enhancement of fluorescence emission, improved fluorophore photostability, and significant reduction of fluorescence lifetimes have been obtained from high aspect ratio (>100) silver (Ag) nanowires. These quantities are found to depend on the surface loading of Ag nanowires on glass slides, where the enhancement of fluorescence emission increases with the density of nanowires. The surface loading dependence was attributed to the creation of intense electric fields around the network of Ag nanowires and to the coupling of fluorophore excited states that takes place efficiently at a distance of 10 nm from the surface of nanowires, which was confirmed by theoretical calculations. The enhancement of fluorescence emission of fluorescein isothiocyanate (FITC) was assessed by fluorescence spectroscopy and fluorescence-lifetime imaging microscopy (FLIM) to demonstrate the potential of high aspect ratio Ag nanowires. Fluorescence enhancement factors exceeding 14 were observed on Ag nanowires with high loading by FLIM. The photostability of FITC was the highest on nanowires with medium loading under continuous laser excitation for 10 min because of the significant reduction in the fluorescence lifetime of FITC on these surfaces. These results clearly demonstrate the potential of Ag nanowires in metal-enhanced fluorescence-based applications of biosensing on planar surfaces and cellular imaging.



INTRODUCTION

Metal-enhanced fluorescence (MEF) phenomenon is described as the increase in fluorescence emission of fluorescent species due to their close-range interactions with plasmon resonant metal nanoparticles.^{1,2} These interactions occur at distances of 4–200 nm and are a result of nonradiative transfer of energy from the excited state of the fluorescent species to surface plasmons of the metal nanoparticles (i.e., coupling of energies), which is scattered as fluorescence emission by the metal nanoparticles into free space.³ Fluorescence emission from fluorescent species within 0–4 nm of metal nanoparticles is mostly quenched by metal nanoparticles.^{4,5} In addition, an increase in the electric fields between and around the metal nanoparticles because of plasmon–plasmon interactions can increase the extent of absorption of light by fluorescent species.^{3,6} Subsequently, while the overall fluorescence emission from the metal nanoparticle–fluorescent species system is increased significantly, the fluorescent species spend less time in their excited states (i.e., their lifetimes can be reduced) and emit fluorescence for a longer time (improved photostability).^{7,8} There are two major factors that affect the efficiency of the metal particle–fluorophore interactions: (1) size and type of the metal nanoparticles⁹ and (2) the wavelength of emission of fluorophores.¹⁰ It was previously described that the MEF phenomenon is related to absorption and scattering components of the metal nanoparticles and that

the size of the metal nanoparticles play a critical role in the energy transfer from the fluorescent species to the metal nanoparticles.^{3,11–13} For example, the use of metal nanoparticles smaller than 40 nm can result in quenching of fluorescence emission,¹⁴ and the use of metal nanoparticles larger than 40 nm can enhance the fluorescence emission of fluorescent species.^{15,16} In addition, the most efficient nonradiative energy transfer from fluorescent species at their excited states to surface plasmons of metal nanoparticles occurs when there is a spectral overlap between the fluorescence emission of the fluorescent species and the dominant surface resonances of metal nanoparticles.¹⁴

On the basis of the observed benefits of the MEF phenomenon described above, metal nanoparticles are employed in several fluorescence-based applications, such as immunoassays,¹⁷ fluorescence *in situ* hybridization assays, and tracking of cellular mechanisms.^{18–25} In these applications, fluorophores with high quantum yields are typically employed to increase the detectability of fluorescent emission, which can result in high background emission and poor fluorophore photostability. The use of metal nanoparticles (such as silver,²⁶ gold,²⁷ copper,²⁸ or aluminum²⁹) in these applications afford

Received: September 6, 2014

Revised: November 7, 2014

Published: December 10, 2014

for the use of low quantum yield fluorophores, which can withstand prolonged exposure to excitation light so that multiple measurements can be made. The size of these metal nanoparticles can go up to 200 nm, which are randomly deposited as nanostructures of various shapes (islands, triangles, spheres, fractals, etc.) or precisely controlled arrays on planar surfaces. The preparation of randomly deposited metal nanoparticles can be achieved in solution or by electrochemical means and is relatively simpler than preparation of precisely controlled arrays that require sophisticated instrumentation. Precisely controlled arrays yield narrower surface plasmon resonances, which affords for better control of the scattered light and the optimization of spectral overlap between the fluorescent species and the surface resonances of metal nanoparticles.³⁰

In addition to metal nanoparticles mentioned above, noble metal nanowires are predicted, and in few occasions demonstrated, to create an alternative surface in MEF-based applications.^{31,32} Earlier theoretical simulations by Schatz et al.³⁰ showed that metal nanowires can generate intense electromagnetic fields at their ends as compared to other shapes. In addition, Olejnik et al.³³ have reported the enhancement of fluorescence intensity of chlorophyll molecules embedded in protein complexes coupled with Ag nanowires. They demonstrated that the enhancement of fluorescence emission was because of the interaction between excited states of chlorophyll-containing photosynthetic complexes and plasmon excitations in Ag nanowires.³³ However, 2-fold increase of the emission intensity was observed for complexes located at the ends of the nanowires, which was attributed to antennae effect, in which higher density of electromagnetic field is usually expected for structures with high curvature.³³ Moreover, Ag nanowires have also been demonstrated to strongly enhance the absorption of poly(3-hexylthiophene) (P3HT), which can be applied in improving the efficiency of organic solar cells.³⁴ Furthermore, Goldys et al.^{31,32} have reported enhanced fluorescence emission from fluorophores placed within 4 nm of the high aspect ratio Ag and gold nanowire surfaces using fluorescein isothiocyanate (FITC)—albumin, which was attributed to the coupling of fluorescence emission to surface plasmons and enhanced electric fields around the tip of the nanowires. However, because of the nature of the synthesis of Ag nanowires via an electrochemical method, nanowires with fractal architecture were deposited in a heterogeneous manner and used for the measurements. Therefore, the enhancement of fluorescence by the Ag nanowire fractals was not uniform throughout the surface and varied depending on the thickness of Ag nanowire fractals. The lifetime of fluorophores was reported to decrease significantly and also was dependent on the thickness of Ag nanowire fractals; however, the photostability of fluorophores were not investigated.³¹ Although the enhancement of fluorescence emission coupled with decreased lifetimes is important to demonstrate the MEF phenomenon, the demonstration of improved photostability of fluorophores is critical in successful application of MEF phenomenon in biosensing and cellular imaging applications.

We present the complete investigation for the use of surface-bound Ag nanowires with aspect ratio larger than 100 synthesized by a polyol method to show high enhancement of fluorescence emission, improved fluorophore photostability, and significant reduction of fluorescence lifetimes. To demonstrate that our deposition technique can be used to

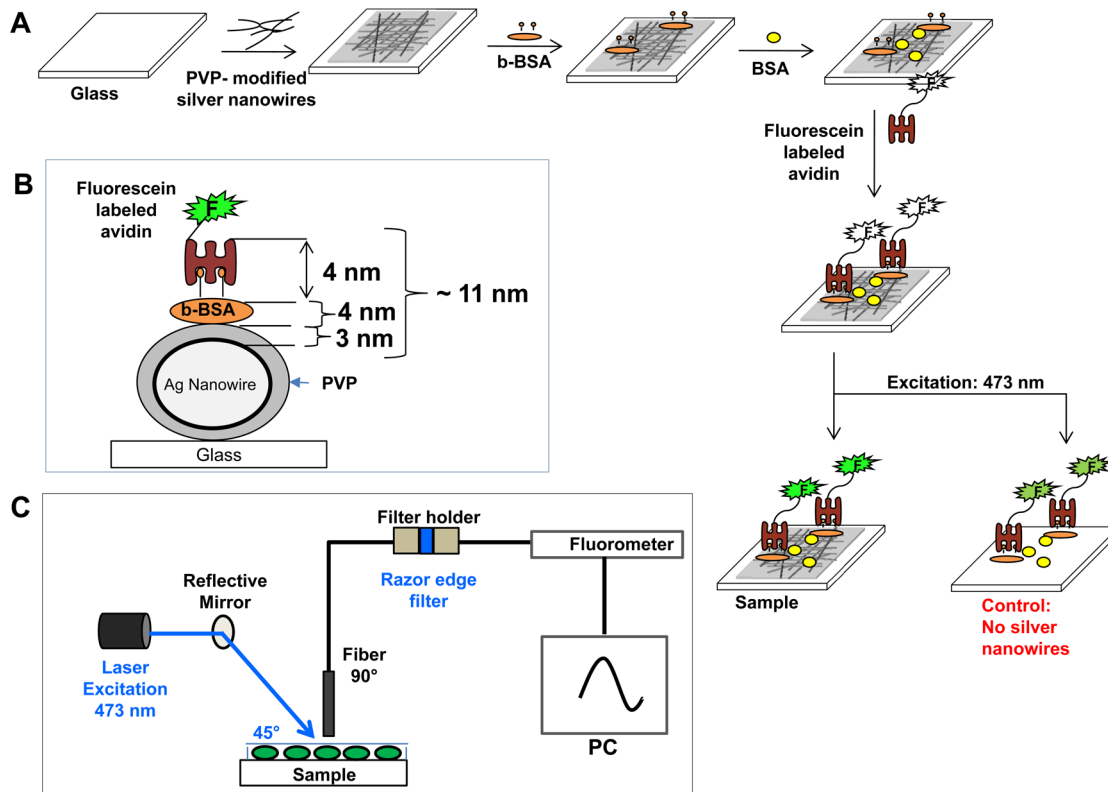
control the extent of Ag nanowires on glass slides, three different surface densities containing 0.33, 0.62, and 0.99 nanowires/ μm^2 were prepared in a homogeneous fashion via spray coating. On the basis of our theoretical calculations, the largest predicted increase in the electric field around the Ag nanowires was \sim 10 nm away from the Ag surface. In this regard, to maximize the efficiency of the interactions of excited state of the fluorescent species with the surface plasmons of the metal nanoparticles in the presence of the increased electric fields, we have designed a biotinylated albumin–FITC-labeled avidin-based bioassay to place the fluorescent species (FITC) at \sim 11 nm. Fluorescence emission spectroscopy and fluorescence-lifetime imaging microscopy (FLIM) techniques were employed to demonstrate the use of high aspect ratio Ag nanowires in potential MEF-based applications for biosensing on planar surfaces and cellular imaging, respectively. Fluorescence enhancement factors up to \sim 14.3 were observed on Ag nanowires with high loading by FLIM. The photostability of FITC was significantly improved on Ag nanowires with medium loading under continuous laser excitation for 10 min because of the reduction in the fluorescence lifetime of FITC from 0.94 ns on blank glass slides to 0.51 ns on these surfaces.

EXPERIMENTAL SECTION

Materials. FITC-labeled avidin, bovine serum albumin (BSA), biotinylated bovine serum albumin (b-BSA), silicon isolator (12 well, 2.0 mm diameter, 1.5 mm deep), ethylene glycol (EG), silver nitrate (AgNO_3), poly(vinylpyrrolidone) (PVP, MW = 55 000 g/mol), and sodium chloride (NaCl) were all obtained from Sigma-Aldrich and used without further purification. All aqueous solutions were prepared using deionized water ($>18.0 \text{ M}\Omega\cdot\text{cm}$ resistivity at 25 °C) obtained from a Millipore Direct Q3 system except when stated otherwise.

Methods. Synthesis and Deposition of Ag Nanowires onto Glass Slides. Synthesis of Ag nanowires and their following deposition onto glass slides were achieved according to the procedure reported elsewhere.³⁵ In the synthesis process, 10 mL of 0.45 M ethylene glycol solution of PVP (monomer-based calculation MW = 55 000 g/mol) was prepared, then 7 mg of NaCl (99.5%) was added into the polymer solution. The PVP/EG solution was then heated to 170 °C. A separate AgNO_3 solution in 5 mL of EG was then prepared and added dropwise to the PVP/EG solution using an injection pump (Top-5300 model syringe pump) at a rate of 5 mL/h. The solution was then annealed for another 30 min at 170 °C and later air-cooled to room temperature. To purify the synthesized Ag nanowires, the solution was diluted with acetone (in a ratio of 1:5) and centrifuged twice at 8000 rpm for 20 min. Nanowires were then dispersed in ethanol and centrifuged for a second time at 8000 rpm for 20 min. The final product was then dispersed in ethanol. The deposition of Ag nanowires from ethanolic solutions to glass substrates was made possible by spray coating. To obtain Ag nanowire networks with different densities, the number of spraying steps was increased. The Ag nanowire-deposited glass slides were then placed on a hot plate heated to 130 °C for instant evaporation of ethanol. As-coated Ag nanowires were used directly in MEF studies and were annealed at 200 °C for 20 min for the removal of residual PVP from lateral surfaces of nanowires to be used only in scanning electron microscopy (SEM) analysis. ImageJ (soft-

Scheme 1. Schematic Depiction of (A) Metal-Enhanced Fluorescence from FITC-Labeled Avidin Immobilized on Ag Nanowire-Deposited Glass Slides Using b-BSA, (B) the Distance between the Ag Nanowires and FITC, and (C) Experimental Setup for Metal-Enhanced Fluorescence Studies Based on Fluorescence Emission Spectrum Measurements



ware developed by National Institutes of Health) was used for the network density calculations.

Preparation of the Protein Assay (Biotin–Avidin) on Ag Nanowire-Deposited Glass and on Blank Glass Slides (Control Assay). The procedure for the preparation of the model assay was adopted from previously published papers based on the binding of b-BSA onto Ag and glass surfaces.^{36,37,11} Scheme 1A summarizes the steps involved in the preparation of protein assay on all surfaces, where fluorophores are placed ~11 nm away from the Ag surface (Scheme 1B). Biotin groups were introduced to the surface by the employment of b-BSA, before the binding of FITC-labeled avidin via specific interactions of biotin and avidin, which forms a monolayer on the Ag nanowires and blank glass slides (control surface). The binding of b-BSA (~30 μL) to Ag nanowires and blank glass covered with a silicon isolator was accomplished by incubating 10 μM of b-BSA in a pH 7 buffer for approximately 30 min, which was then washed using buffer solution to remove unbound materials and dried using air. BSA solution (~30 μL, 0.5 mg/mL) was then incubated within the chambers of the silicon isolator for 30 min to minimize nonspecific binding of FITC-labeled avidin onto the surfaces. FITC-labeled avidin was prepared using PBS buffer solution at a pH of 7, and the stock solution was diluted to achieve a final concentration of 1 μM. Subsequently, 30 μL of 1 μM of FITC-labeled avidin was then added into the b-BSA-coated Ag nanowire-deposited and blank glass for 30 min at room temperature (20 °C).

Fluorescence Measurements and Real-Color Images. In this investigation, all fluorescence emission spectra were measured using an in-house build setup for fluorescence

spectroscopy, equipped with a Fiber Optic Spectrometer (Jaz, Ocean Optics, Inc., FL, U.S.A.), a laser 473 nm (BW&Tek, Inc., DE, U.S.A.), fiber optic connections and reflective mirrors as shown in Scheme 1C). Samples were excited at a 45° angle and the fluorescence emission was detected through a 473 nm razor-edge emission filter (Thorlabs, USA). In addition, all fluorescence measurements were carried out in 2 min while the laser beam was blocked in between measurements (actual laser exposure time is ~4 s for each measurement), to minimize the photodestruction of the fluorophores. In this regard, fluorescence measurements are consistent with respect to laser exposure and detection periods. Real-color images of FITC-labeled avidin on Ag nanowire-deposited and blank glass were taken with an 8 MP digital camera through the same emission filter as used to record the emission spectra.

Photostability Experiments. The photostability of FITC was accomplished at 473 nm using continuous laser excitation for 600 s.

Fluorescence Lifetimes. All fluorescence lifetime measurements for fluorescein-labeled avidin on Ag nanowire-deposited and blank glass slides were performed (Center for Fluorescence Spectroscopy, University of Maryland School of Medicine, Baltimore, MD, U.S.A.) using a PicoQuant Single-Molecule Scanner (Berlin, Germany) mounted on an Olympus IX71 inverted microscope (Tokyo, Japan) with an Olympus LCPLFL 20× objective lens and numerical aperture of 0.40. The fluorescence lifetimes for all samples were determined at room temperature on glass substrates. In addition, the image area was 200 × 200 μm with frames (4× average) of 256 × 256 pixels. Intensity values were measured with 2 ms dwell times, and the

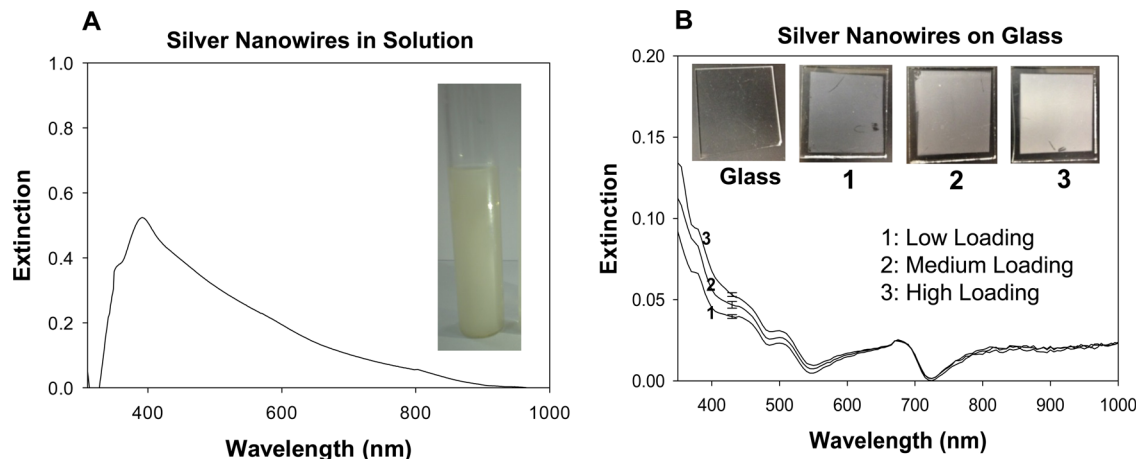


Figure 1. Absorbance spectra of (A) Ag nanowires in solution (inset, real-color photograph of Ag nanowires solution before the spray coating process) and (B) blank glass slide and Ag nanowires (low, medium, and high loading) deposited onto glass slides (inset, real-color photographs of Ag nanowires on glass slides).

lifetimes were determined over an average area at 1 ms dwell times.

Theoretical Simulations. COMSOL Multiphysics was employed to simulate the electric field distributions around Ag nanowires, multiple array configurations of Ag nanowires with an average diameter and length of 72 nm and $\sim 10 \mu\text{m}$, respectively (based on finite element method to solve Maxwell's equation for a coupled emitter–nanowire system, version 4.3b with RF module). [Note: the wavelength of the light source was selected to be 520 nm, similar to the fluorescence emission wavelength of FITC.] In this regard, Ag nanowires were simulated in a single line of horizontal and vertical, and horizontal (2×3) and vertical (3×2) array formats to predict the coupling of fluorescence emission to translational mode of surface plasmon (shown in Figure 4C). The horizontal (2×3) and vertical (3×2) array format was simulated to investigate the SPR effect at the Ag nanowire junctions formed by overlapping deposition as compared to that of a single nanowire.

RESULTS AND DISCUSSION

The Ag nanowires were synthesized using a solution-based polyol process.^{38,39} To demonstrate the utilization of PVP-modified Ag nanowires in MEF-based applications on solid platforms, these nanowires were deposited onto glass slides. The loading of the Ag nanowires on glass slides was changed by the number of spraying steps. Figure 1A shows the absorbance spectrum (380–1000 nm) of Ag nanowires in ethanol solution. A dominant surface plasmon resonance peak (SPR) peak at a wavelength of ~ 380 nm for Ag nanowires in solution was observed, which is consistent with typical optical properties of Ag nanowires synthesized via the polyol process.⁴⁰ The SPR peak at 380 nm corresponds to the transverse SPR mode of the Ag nanowires.⁴¹ However, no longitudinal SPR mode for Ag nanowires in solution was observed within the wavelength range of 380–1000 nm, implying the presence of significantly large (>100) aspect ratio Ag nanowires. It is important to note that the wavelength range of 380–1000 nm studied here overlaps with the range of emission wavelengths of most commercially available fluorophores for MEF applications. Therefore, it is thought that the longitudinal SPR peak (>1000 nm) has no effect on the fluorescence emission of fluorophores. In addition to the observations described above, the absorption

spectrum of Ag nanowires in solution displayed broadening, which can be attributed to the coupling of the SPR due to the decrease in spacing between the nanowires. The inset of Figure 1A shows the real-color photograph of Ag nanowires in solution before their use in the spray coating process. The Ag nanowire solution is a cloudy yellow-green, a typical color of Ag colloids with a dominant transverse SPR peak around 400 nm.

Ag nanowires deposited onto glass slides were also characterized by optical spectroscopy. Figure 1B shows the absorbance spectrum (380–1000 nm) of Ag nanowires (i.e., low, medium, and high loading) on glass slides with their respective standard deviation at ~ 430 nm, which shows the reproducibility of the Ag nanowires, and the inset shows their real-color photographs. A blank glass slide was used as the control surface and is shown to demonstrate the change in the color of glass slides following the deposition of Ag nanowires with different surface loading. The color of the glass slides changes from transparent to opaque as the loading of the Ag nanowires on glass slides increases. The dominant transverse SPR peak for Ag nanowires on glass slides appears around 380 nm. Similar to Ag nanowires in solution, the longitudinal SPR peak for Ag nanowires on glass slides was not observed. The observed minimum in absorption spectrum at 720 nm can be attributed to the change in the dielectric constant of the surface due to the presence of PVP and is not related to surface plasmons.

In addition to the characterization of optical features of the Ag nanowires described above, SEM was employed to quantify the extent of loading of Ag nanowires on glass slides and to visualize the surface features of the glass slides; the results are shown in Figure 2 and Figure S1 in Supporting Information. SEM images of Ag nanowires on glass slides show that the average diameter and length of Ag nanowires for all surfaces was ~ 72 nm and $\sim 10 \mu\text{m}$, respectively. The average aspect ratio (i.e., length/diameter) of the nanowires is then calculated to be greater than 100. The thickness of the PVP coating on the nanowires was measured to be ~ 3 nm for all surfaces (Figure 2B inset). The Ag nanowire loading on glass slides was calculated to be (i) $0.33 \text{ nanowires}/\mu\text{m}^2$ for low loading, (ii) $0.62 \text{ nanowires}/\mu\text{m}^2$ for medium loading, and (iii) $0.99 \text{ nanowires}/\mu\text{m}^2$ for high loading. SEM images also show that Ag nanowires form a network composed of individual nanowires without any apparent aggregation. However, nano-

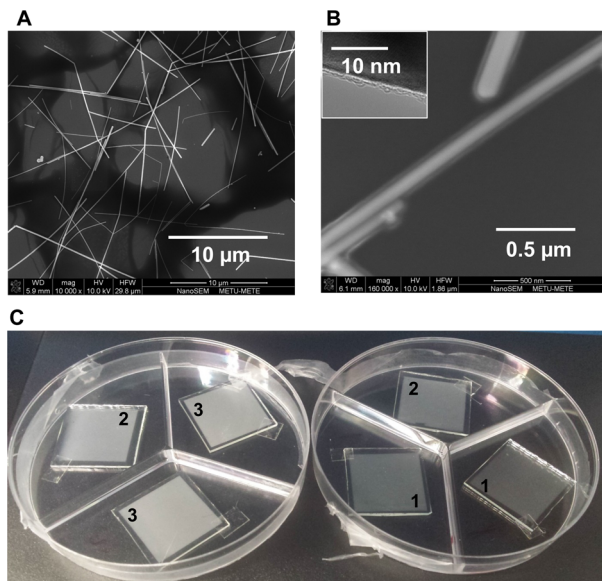


Figure 2. Low-resolution (A) and high-resolution (B) SEM images of as-deposited Ag nanowire networks on glass slides. (C) Real-color photographs of Ag nanowires on glass substrates to demonstrate the reproducibility of the surfaces.

wires appeared to overlap on several contact points on the samples even for the low loading (Figure 2A and Figure S1A in Supporting Information). As the loading of Ag nanowires was increased, the number of contact points between the nanowires increase, which can result in the increased electric fields near the contact points. Therefore, the fluorescence emission of

fluorophores located at the contact points can be significantly enhanced because of coupling of surface plasmons, which is the crux of the use of Ag nanowire networks with high aspect ratio in MEF applications. It is also important to note that the spray coater employed in this work for the deposition of Ag nanowires onto glass slides yields highly reproducible surfaces (Figure 2C), which is critically important for quantitative applications of MEF.

To elucidate the coupling of fluorescence emission to translational mode of surface plasmons for Ag nanowires, theoretical simulations were carried out for various interparticle distances using COMSOL Multiphysics. In this regard, several types of configurations of Ag nanowires on glass slides were considered based on our SEM images, where nanowires were either stacked side-by-side (horizontally) or vertically, as depicted in Figure 3. The distance between the individual Ag nanowires was varied between 6 and 1000 nm to simulate all potential configurations of nanowires on the surface, i.e., a distance of 6 nm corresponds to two Ag nanowires overlapping (vertically) or placed side-by-side (horizontally) on the glass slides without any separation. It is important to note that each Ag nanowire has a \sim 3 nm thick PVP coating, and the closest distance between the two Ag nanowires with PVP is \sim 6 nm. Figure 3A,B shows the largest predicted electric field intensity (E_z) versus interparticle distance (6–1000 nm) for all configurations of the Ag nanowire networks. Figure 3A,B also shows that the largest value of electric field intensity was predicted to occur at a distance of 10 nm between the Ag nanowires for all configurations. Figure 3C shows the electric field distribution for Ag nanowire networks with an interparticle distance of 10 nm. The electric field intensity is predicted to

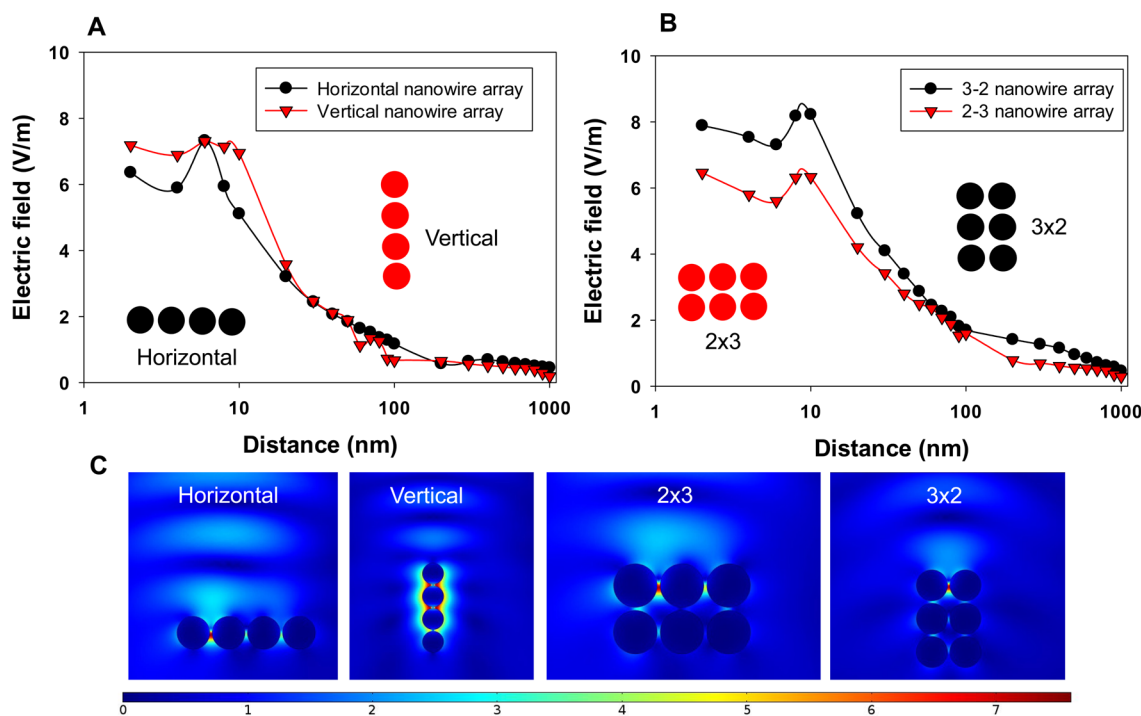


Figure 3. Electric field intensity (largest predicted value) versus the distance of Ag nanowires using COMSOL Multiphysics: (A) Ag nanowires @ horizontal and vertical array format and (B) Ag nanowires @ horizontal (2×3) and vertical (3×2) array format to predict the coupling of fluorescence emission (520 nm) to translational mode of surface plasmons. (C) The electric field (E_z) density distribution over the translational cross section of Ag nanowires (the distances between the nanowires are 10 nm). In this configuration, the wavelength of the light source is 520 nm, similar to the fluorescence emission wavelength of FITC, which is expected to be \sim 11 nm from the Ag nanowires in all directions, as depicted in Scheme 1

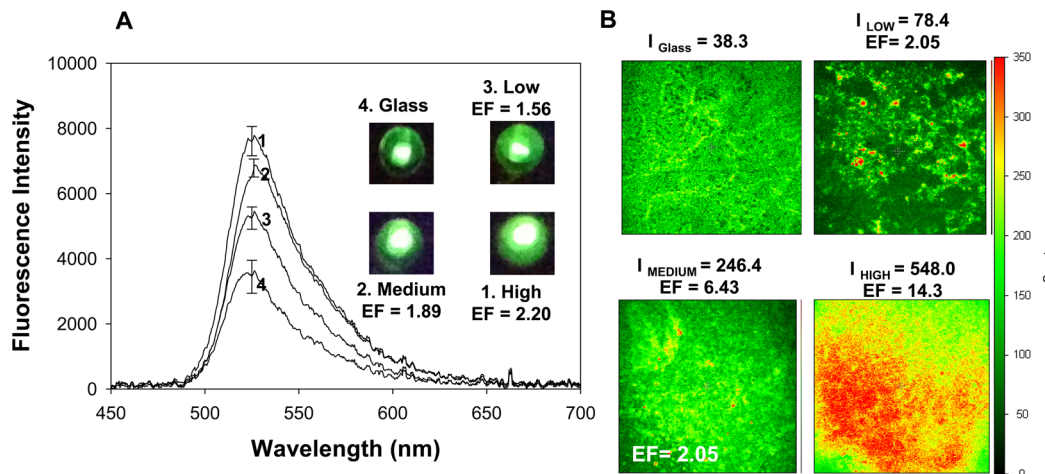


Figure 4. (A) Emission spectrum of fluorescein-labeled avidin on Ag nanowire-deposited glass slides (low, medium, and high loading) and control sample (blank glass slide). Inset: real-color photographs of fluorescence emission from surfaces prepared on the different platforms and control experiments. The measurements were the mean spectra of five separate surface locations for three different runs. (B) Fluorescence emission measurements of fluorescein-labeled avidin on Ag nanowire-deposited glass slides and control sample of $2 \times 2 \text{ mm}^2$ area using FLIM with a dwell time of 1 ms. Emission, $514 \pm 30 \text{ nm}$; objective, $20\times$; NA, 0.4; I, intensity, arbitrary units. Excitation for both types of measurements, 473 nm; EF, enhancement factor = intensity value of Ag nanowires divided by intensity value on blank glass.

have the largest value between the individual Ag nanowires and decreases significantly at locations beyond nanowires. These predictions imply that the coupling of the excited states of the fluorophores to surface plasmons of Ag nanowires occurs mainly when they are located within $\sim 10 \text{ nm}$ of each other. It is also interesting to note that the predicted increases in the electric field intensities are similar for both the horizontal and vertical configurations of Ag nanowire networks, which implies that the variation of average measured fluorescence emission intensities from these surfaces should be minimal. Therefore, MEF-based applications of Ag nanowire networks are expected to yield homogeneous fluorescence measurements throughout the surface, which is critical for the reproducibility of these applications.

To demonstrate the proof-of-principle use of Ag nanowires in MEF-based applications, nanowires were coated with b-BSA (model protein of interest) and FITC-labeled avidin (the detector protein).¹¹ In this regard, the following two detection techniques were employed: (1) fluorescence spectroscopy for biosensing applications based on planar surfaces and (2) FLIM for applications that require fluorescence measurements from a small area. Figure 4A shows the summary of the results of the fluorescence emission spectra of FITC measured from Ag nanowire-deposited glass slides (low, medium, and high loading). A control experiment with blank glass was also carried out to assess the effect of Ag nanowires on the fluorescence emission of FITC. It is important to note that the fluorescence emission spectra of FITC were collected from the randomly selected points with $\sim 2 \text{ mm}$ diameter on the surfaces exposed to laser excitation. Subsequently, the fluorescence emission was averaged over the area of the laser spot (as shown in the inset of Figure 4A, real-color photographs of fluorescence emission taken through an emission filter from the Ag nanowires and glass surfaces). In this configuration, the fluorescence emission spectrum is collected by a fiber optic detector placed 1 cm from the surface, which results in the inclusion of lower emission values from the darker area surrounding the laser spot. Figure 4A shows that the emission intensity of FITC at 520 nm increases as the loading of the Ag nanowire networks increases on the glass surface. The

enhancement factor (EF) of fluorescence intensity (arbitrary units) on Ag nanowires was calculated as the intensity values of nanowires divided by the intensity values observed on the control samples, and the results are provided in the inset of Figure 4A for (i) low loading (EF = 1.56), medium loading (EF = 1.89), and high loading (EF = 2.20). The experimental configuration employed here is typically used in MEF-based biosensing applications carried out on planar substrates.^{36,42–46}

It is important to comment on the relevance of theoretical calculations (Figure 3) to the experimental fluorescence data presented in Figure 4. We note that the theoretical simulations were used to elucidate the coupling of fluorescence emission to the translational mode of surface plasmons for Ag nanowires in terms of electric field distribution around the Ag nanowires created by a single-wavelength light source at 520 nm. These predictions revealed that the coupling of the excited states of the fluorophores to surface plasmons of Ag nanowires occurs mainly when they are located within $\sim 10 \text{ nm}$ of each other. On the other hand, the data presented in Figure 4 is from the coupling of fluorescence emission of 500–600 nm (Figure 4A) to Ag nanowires. It is thought that the increased electric fields around nanowires facilitate the coupling of fluorescence emission to surface plasmons of Ag nanowires. We also note that the predicted values in Figure 3 are for electric field (volts per meter) and the fluorescence enhancement factors shown in Figure 4 are dimensionless (intensity (counts per second) on Ag divided by intensity on glass (counts per second)). Therefore, there is no direct correlation between volts per meter and the dimensionless enhancement factor.

To investigate the effect of Ag nanowires on fluorescence emission from a smaller area ($\sim 2 \times 2 \mu\text{m}^2$) for localized events, such as tracking of cellular mechanisms,^{18–24} the fluorescence emission intensity of FITC at $514 \pm 30 \text{ nm}$ was measured using FLIM with a dwell time of 1 ms (Figure 4B). The fluorescence emission intensity on glass was measured as 38.3 (arbitrary units, a.u.; Ag nanowires with low loading, 78.4 (a.u.); medium loading, 246.4 (a.u.); high loading, 548.0 (a.u.)). The enhancement factor for fluorescence emission from the Ag nanowires was calculated as 2.05, 6.43, and 14.3 for low, medium, and high loading, respectively. These observations can be attributed to

the increased coupling of fluorescence emission to the surface plasmons of Ag nanowires, where the extent of coupling is directly related to the loading of nanowires in close proximity to the fluorophores.^{31,32} In this regard, as the loading of Ag nanowires on the surface is increased and the extent of contact points between the overlapping nanowires is increased, the coupled emission can extend to neighboring nanowires, which can in turn produce new channels for energy transfer and subsequently increase the fluorescence signal.^{31,32} It is also important to comment on the extent of protein present on blank glass and silvered surfaces, which can contribute to the enhancement of fluorescence on silvered surfaces because of the differences between the surface area of both surfaces. Our research group has previously reported that the extent of proteins on silvered surfaces (50–90 nm in diameter) and blank glass slides are similar.^{47–49} Therefore, the potential contribution of increased surface area on silvered surface to the enhancement of fluorescence was deemed to be insignificant as compared to the effect of surface plasmons on fluorescence emission.

In MEF-based applications, the detectability of the fluorescence emission is also affected by the photostability of the fluorophores.⁵⁰ In this regard, the photostability of FITC adsorbed onto Ag nanowires as compared to a glass surface was investigated, and the results can be seen in Figure 5. Figure 5A shows the raw data for fluorescence emission from FITC-

labeled avidin on Ag nanowire-deposited glass slides and control samples as a function of time. The emission intensity of FITC on blank glass slides (initial value ~3109) was decreased by 26% after 10 min of continuous laser excitation (final value ~2308), while the decrease in fluorescence emission intensity of FITC was 22%, 22%, and 28% for Ag nanowires with low, medium, and high loading, respectively. Figure 5B shows the time progression of the decrease in the normalized fluorescence emission intensity of FITC as described above. Figure 5B also shows that the fluorescence emission of FITC decreases the fastest on glass slides and the slowest on Ag nanowires with low loading (i.e., 0.33 nanowires/ μm^2). To explain these observations from the perspective of total number of photons detected from each surface for the duration of 10 min, the area under each curve was calculated. Although the decrease in fluorescence emission intensity of FITC on blank glass slides and Ag nanowires with high loading are similar (Figure 5B), the total number of photons detected from Ag nanowires with high loading (2.10×10^6) is ~2.44-fold greater than the total number of photons detected from blank glass slides (0.86×10^6). These results imply that the Ag nanowires deposited onto glass slides can increase the detectability of the fluorescence emission from samples as compared to the blank glass slides.

It has been previously shown and discussed in numerous papers on MEF phenomena that the lifetime of fluorophores are also modified when placed in close proximity to Ag nanostructures.^{11,31,51,52} Therefore, we measured the fluorescence lifetime of FITC on all surfaces using FLIM. Figure 6A–D show the fluorescence lifetime image and histogram for FITC adsorbed onto blank glass slides (Figure 6A) and onto Ag nanowires (Figure 6B–D). The average lifetime (τ) for FITC on blank glass slides was measured to be 0.94 ± 0.12 ns, which was significantly reduced on Ag nanowires (low loading, $\tau = 0.62 \pm 0.12$ ns; medium loading, $\tau = 0.51 \pm 0.07$ ns; and high loading, $\tau = 0.60 \pm 0.10$ ns). The largest reduction in fluorescence lifetime of FITC was observed on Ag nanowires with medium loading, which explains the observation of improved photostability on these surfaces. These results provide direct evidence for the coupling of excited-state energies of FITC with the surface plasmons of nanowires with high aspect ratio.

CONCLUSIONS

Ag nanowires with aspect ratio larger than 100 were deposited onto glass slides using a spray deposition method in a homogeneous and reproducible fashion. Nanowire density on the glass surface was varied to generate low, medium, and high levels of loading. The ability of Ag nanowires to enhance the fluorescence emission of a fluorophore placed in close proximity was assessed using fluorescence spectroscopy and FLIM. In this regard, FITC-labeled avidin was placed ~11 nm away from Ag nanowires using biotin–avidin interactions. The fluorescence emission of FITC was enhanced up to ~2.2-fold on Ag nanowires with high loading as compared to a control surface (i.e., blank glass without nanowires) using fluorescence spectroscopy over a surface ~2 mm in diameter. Fluorescence emission measurements on Ag nanowires with high loading and a control sample from a smaller area ($2 \times 2 \mu\text{m}^2$) using FLIM revealed that the enhancement of fluorescence emission of FITC was ~14.3-fold. The variation in the fluorescence emission enhancement factors obtained using fluorescence emission spectroscopy and FLIM was attributed to the experimental setup, which can be used in MEF-based

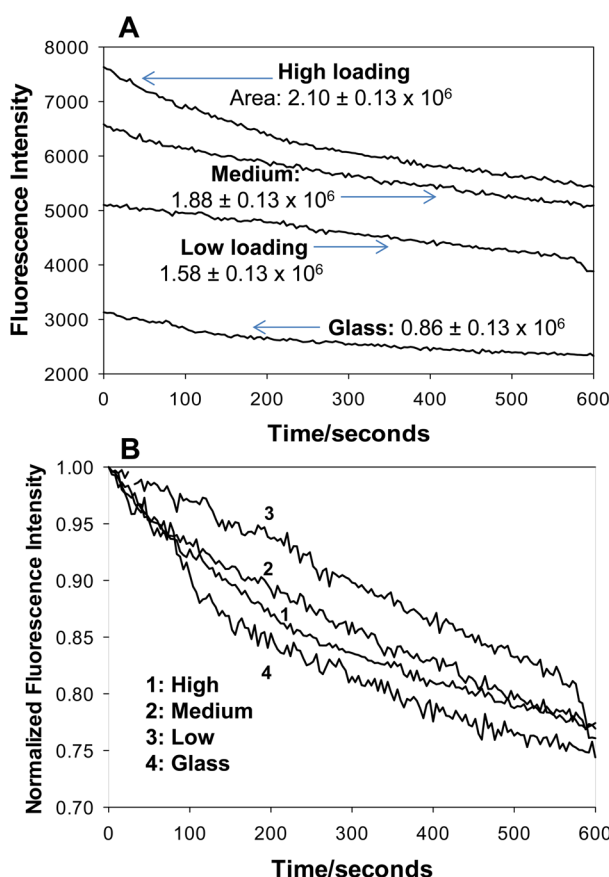


Figure 5. (A) Photostability of fluorescein-labeled avidin on Ag nanowire-deposited glass slides (low, medium, and high loading) and control samples. Note: these values are averages of three different measurements. (B) Normalized fluorescence intensity versus time measured in panel A.

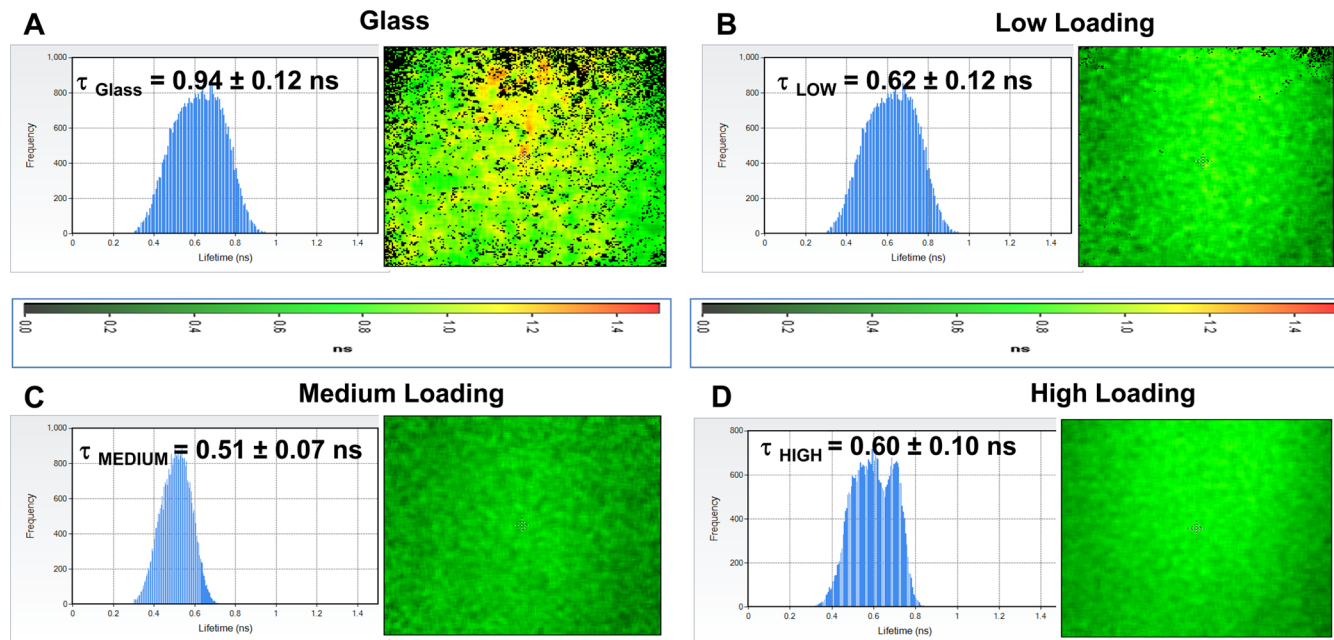


Figure 6. Fluorescence lifetime image and histogram for FITC-labeled avidin on (A) blank glass slides and Ag nanowire-deposited glass slides with (B) low loading, (C) medium loading, and (D) high loading (τ , average lifetime).

biosensing applications on planar platforms and cellular imaging, respectively. In addition, the distance-dependent electric field distribution around Ag nanowires was investigated by theoretical simulations, which indicated that the optimum distance for efficient coupling of fluorescence emission from fluorophores to surface plasmons of Ag nanowires is ~ 10 nm. It was also observed that FITC molecules showed the highest photostability on Ag nanowires with medium loading under continuous laser excitation for 10 min, which can be attributed to the significant reduction in the fluorescence lifetime of FITC on these surfaces. The observations of increased fluorescence intensity, greater fluorophore photostability, and reduced lifetime in the presence of nanowires described in this work prove that MEF from Ag nanowires with high aspect ratio can be observed. Our results simply reveal that Ag nanowires on glass slides can be used as alternative surfaces in MEF-based applications.

ASSOCIATED CONTENT

Supporting Information

Additional SEM images of bare silver nanowire networks with different densities on glass slides. This material is available free of charge via the Internet at <http://pubs.acs.org>.

AUTHOR INFORMATION

Corresponding Authors

*E-mail: Kadir.Aslan@morgan.edu. Phone: (443) 885-4257. Fax: (443) 885-8286

*E-mail: unalan@metu.edu.tr. Phone: +90 312 210 5939. Fax: +90 312 210 2518.

Notes

The authors declare no competing financial interest.

ACKNOWLEDGMENTS

This work was partially supported by Award 5-K25EB007565-05 (K.A.) from the National Institute of Biomedical Imaging and Bioengineering. The content is solely the responsibility of

the authors and does not necessarily represent the official views of the National Institute of Biomedical Imaging and Bioengineering or the National Institutes of Health. H.E.U. acknowledges support by TUBITAK (Grant 109M487) and the Distinguished Young Scientist Award of the Turkish Academy of Sciences (TUBA). S.C. acknowledges support from METU-OYP Project (1439).

REFERENCES

- (1) Geddes, C. D.; Parfenov, A.; Lakowicz, J. R. Photodeposition of Silver Can Result in Metal-Enhanced Fluorescence. *Appl. Spectrosc.* **2003**, *57*, 526–531.
- (2) Deng, W.; Xie, F.; Baltar, H. T.; Goldys, E. M. Metal-Enhanced Fluorescence in the Life Sciences: Here, Now and Beyond. *Phys. Chem. Chem. Phys.* **2013**, *15*, 15695–15708.
- (3) Aslan, K.; Geddes, C. D. Metal-Enhanced Chemiluminescence: Advanced Chemiluminescence Concepts for the 21st Century. *Chem. Soc. Rev.* **2009**, *38*, 2556–2564.
- (4) Drexhage, K. H.; Kuhn, H.; Schäfer, F. P. Variation of the Fluorescence Decay Time of a Molecule in Front of a Mirror. *Ber. Bunsen-Ges.* **1968**, *72*, 329–329.
- (5) Sugawa, K.; Tamura, T.; Tahara, H.; Yamaguchi, D.; Akiyama, T.; Otsuki, J.; Kusaka, Y.; Fukuda, N.; Ushijima, H. Metal-Enhanced Fluorescence Platforms Based on Plasmonic Ordered Copper Arrays: Wavelength Dependence of Quenching and Enhancement Effects. *ACS Nano* **2013**, *7*, 9997–10010.
- (6) Kim, K.; Lee, Y. M.; Lee, J. W.; Shin, K. S. Metal-Enhanced Fluorescence of Rhodamine B Isothiocyanate from Micrometer-Sized Silver Powders. *Langmuir* **2009**, *25*, 2641–2645.
- (7) Malicka, J.; Gryczynski, I.; Fang, J.; Kusba, J.; Lakowicz, J. R. Increased Resonance Energy Transfer between Fluorophores Bound to DNA in Proximity to Metallic Silver Particles. *Anal. Biochem.* **2003**, *315*, 160–169.
- (8) Ray, K.; Lakowicz, J. R. Metal-Enhanced Fluorescence Lifetime Imaging and Spectroscopy on a Modified Sers Substrate. *J. Phys. Chem. C* **2013**, *117*, 15790–15797.
- (9) Yang, B.; et al. Tuning the Intensity of Metal-Enhanced Fluorescence by Engineering Silver Nanoparticle Arrays. *Small* **2010**, *6*, 1038–1043.

- (10) Cade, N. I.; Ritman-Meer, T.; Kwaka, K.; Richards, D. The Plasmonic Engineering of Metal Nanoparticles for Enhanced Fluorescence and Raman Scattering. *Nanotechnology* **2009**, *20*, 285201.
- (11) Aslan, K.; Gryczynski, I.; Malicka, J.; Matveeva, E.; Lakowicz, J. R.; Geddes, C. D. Metal-Enhanced Fluorescence: An Emerging Tool in Biotechnology. *Curr. Opin. Biotechnol.* **2005**, *16*, 55–62.
- (12) Aslan, K.; Geddes, C. D. Metal-Enhanced Fluorescence: Progress Towards a Unified Plasmon-Fluorophore Description. In *Metal-Enhanced Fluorescence*; Geddes, C. D., Ed.; John Wiley & Sons, Inc: Hoboken, NJ, 2010; 1–23.
- (13) Aslan, K.; Holley, P.; Davies, L.; Lakowicz, J. R.; Geddes, C. D. Angular-Ratiometric Plasmon-Resonance Based Light Scattering for Bioaffinity Sensing. *J. Am. Chem. Soc.* **2005**, *127*, 12115–12121.
- (14) Aslan, K.; Perez-Luna, V. H. Quenched Emission of Fluorescence by Ligand Functionalized Gold Nanoparticles. *J. Fluoresc.* **2004**, *14*, 401–405.
- (15) Goldys, E. M.; Drozdowicz-Tomsia, K.; Xie, F.; Shtoyko, T.; Matveeva, E.; Gryczynski, I.; Gryczynski, Z. Fluorescence Amplification by Electrochemically Deposited Silver Nanowires with Fractal Architecture. *J. Am. Chem. Soc.* **2007**, *129*, 12117–12122.
- (16) Xie, F.; Baker, M. S.; Goldys, E. M. Homogeneous Silver-Coated Nanoparticle Substrates for Enhanced Fluorescence Detection. *J. Phys. Chem. B* **2006**, *110*, 23085–23091.
- (17) Van Dyke, K.; Van Dyke, R. *Luminescence Immunoassay and Molecular Applications*. CRC Press: Boca Raton, FL, 1990.
- (18) Szmacinski, H.; Toshchakov, V.; Piao, W.; Lakowicz, J. R. Imaging of Protein Secretion from a Single Cell Using Plasmonic Substrates. *BioNanoScience* **2013**, *3*, 30–36.
- (19) Huang, Q.; Huang, Z.; Meng, G.; Fu, Y.; Lakowicz, J. R. Plasmonic Nanorod Arrays for Enhancement of Single-Molecule Detection. *Chem. Commun. (Cambridge, U.K.)* **2013**, *49*, 11743–11745.
- (20) Fu, Y.; Zhang, J.; Nowaczyk, K.; Lakowicz, J. R. Enhanced Single Molecule Fluorescence and Reduced Observation Volumes on Nanoporous Gold (NPG) Films. *Chem. Commun. (Cambridge, U.K.)* **2013**, *49*, 10874–10876.
- (21) Akbay, N.; Ray, K.; Chowdhury, M. H.; Lakowicz, J. R. Plasmon-Controlled Fluorescence and Single DNA Strand Sequencing. *Proc. SPIE* **2012**, *8234*, 82340M.
- (22) Toshchakov, V. Y.; Szmacinski, H.; Couture, L. A.; Lakowicz, J. R.; Vogel, S. N. Targeting TLR4 Signaling by TLR4 Toll/IL-1 Receptor Domain-Derived Decoy Peptides: Identification of the TLR4 Toll/IL-1 Receptor Domain Dimerization Interface. *J. Immunol.* **2011**, *186*, 4819–27.
- (23) Zhang, J.; Fu, Y.; Li, G.; Nowaczyk, K.; Zhao, R. Y.; Lakowicz, J. R. Direct Observation to Chemokine Receptor 5 on T-Lymphocyte Cell Surface Using Fluorescent Metal Nanoprobes. *Biochem. Biophys. Res. Commun.* **2010**, *400*, 111–6.
- (24) Szmacinski, H.; Ray, K.; Lakowicz, J. R. Metal-Enhanced Fluorescence of Tryptophan Residues in Proteins: Application toward Label-Free Bioassays. *Anal. Biochem.* **2009**, *385*, 358–64.
- (25) Difilippantonio, M.; Ried, T. *Technicolor Genome Analysis*; Kluwer Academic Publishers/Plenum Press: New York, 2003; Vol. 7, pp 291–316.
- (26) Aslan, K.; Gryczynski, I.; Malicka, J.; Matveeva, E.; Lakowicz, J. R.; Geddes, C. D. Metal-Enhanced Fluorescence: An Emerging Tool in Biotechnology. *Curr. Opin. Biotechnol.* **2005**, *16*, 55–62.
- (27) Aslan, K.; Malyn, S. N.; Geddes, C. D. Metal-Enhanced Fluorescence from Gold Surfaces: Angular Dependent Emission. *J. Fluoresc.* **2007**, *17*, 7–13.
- (28) Zhang, Y. X.; Aslan, K.; Previte, M. J. R.; Geddes, C. D. Metal-Enhanced Fluorescence from Copper Substrates. *Appl. Phys. Lett.* **2007**, *90*, 173116.
- (29) Ray, K.; Szmacinski, H.; Lakowicz, J. R. Enhanced Fluorescence of Proteins and Label-Free Bioassays Using Aluminum Nanostructures. *Anal. Chem.* **2009**, *81*, 6049–54.
- (30) Hao, E.; Schatz, G. C. Electromagnetic Fields around Silver Nanoparticles and Dimers. *J. Chem. Phys.* **2004**, *120*, 357–66.
- (31) Goldys, E. M.; Drozdowicz-Tomsia, K.; Xie, F.; Shtoyko, T.; Matveeva, E.; Gryczynski, I.; Gryczynski, Z. Fluorescence Amplification by Electrochemically Deposited Silver Nanowires with Fractal Architecture. *J. Am. Chem. Soc.* **2007**, *129*, 12117–12122.
- (32) Drozdowicz-Tomsia, K.; Goldys, E. M. Gold and Silver Nanowires for Fluorescence Enhancement. In *Nanowires-Fundamental Research*; Hashim, A., Ed.; 2011; p 315.
- (33) Olejnik, M.; Krajnik, B.; Kowalska, D.; Twardowska, M.; Czechowski, N.; Hofmann, E.; Mackowski, S. Imaging of Fluorescence Enhancement in Photosynthetic Complexes Coupled to Silver Nanowires. *Appl. Phys. Lett.* **2013**, *102*, 083703.
- (34) Smolarek, K.; Ebenhoch, B.; Czechowski, N.; Prymaczek, A.; Twardowska, M.; Samuel, I. D.; Mackowski, S. Silver Nanowires Enhance Absorption of Poly (3-hexylthiophene). *Appl. Phys. Lett.* **2013**, *103*, 203302.
- (35) Coskun, S.; Aksoy, B.; Unalan, H. E. Polyol Synthesis of Silver Nanowires: An Extensive Parametric Study. *Cryst. Growth Des.* **2011**, *11*, 4963–4969.
- (36) Aslan, K.; Geddes, C. D. Microwave-Accelerated Metal-Enhanced Fluorescence: Platform Technology for Ultrafast and Ultrabright Assays. *Anal. Chem.* **2005**, *77*, 8057–8067.
- (37) Aslan, K.; Holley, P.; Geddes, C. D. Microwave-Accelerated Metal-Enhanced Fluorescence (MAMEF) with Silver Colloids in 96-Well Plates: Application to Ultra Fast and Sensitive Immunoassays, High Throughput Screening and Drug Discovery. *J. Immunol. Methods* **2006**, *312*, 137–147.
- (38) Zhang, S.-H.; Jiang, Z.-Y.; Xie, Z.-X.; Xu, X.; Huang, R.-B.; Zheng, L.-S. Growth of Silver Nanowires from Solutions: A Cyclic Penta-Twinned-Crystal Growth Mechanism. *J. Phys. Chem. B* **2005**, *109*, 9416–9421.
- (39) Zhang, W.; Chen, P.; Gao, Q.; Zhang, Y.; Tang, Y. High-Concentration Preparation of Silver Nanowires: Restraining in Situ Nitric Acidic Etching by Steel-Assisted Polyol Method. *Chem. Mater.* **2008**, *20*, 1699–1704.
- (40) Goh, M. S.; Lee, Y. H.; Pedireddy, S.; Phang, I. Y.; Tjiu, W. W.; Tan, J. M. R.; Ling, X. Y. A Chemical Route to Increase Hot Spots on Silver Nanowires for Surface-Enhanced Raman Spectroscopy Application. *Langmuir* **2012**, *28*, 14441–14449.
- (41) Sun, Y. Conversion of Ag Nanowires to AgCl Nanowires Decorated with Au Nanoparticles and Their Photocatalytic Activity. *J. Phys. Chem. C* **2010**, *114*, 2127–2133.
- (42) Aslan, K. Rapid Whole Blood Bioassays Using Microwave-Accelerated Metal-Enhanced Fluorescence. *Nano Biomed. Eng.* **2010**, *2*, 1–9.
- (43) Aslan, K. Rapid and Sensitive Detection of Troponin I-T-C Complex from Human Serum Using Microwave-Accelerated Metal-Enhanced Fluorescence. *Nano Biomed. Eng.* **2011**, *3*, 179–183.
- (44) Aslan, K.; Baillie, L.; Geddes, C. Ultra Fast and Sensitive Detection of Biological Threat Agents Using Microwaves, Nanoparticles and Luminescence. *Journal of Medical, Chemical, Biological, and Radiological Defense* **2010**, *8*, 1–21.
- (45) Aslan, K.; Grell, T. A. J. Rapid and Sensitive Detection of Troponin I in Human Whole Blood Samples by Using Silver Nanoparticle Films and Microwave Heating. *Clin. Chem. (Washington, DC, U.S.)* **2011**, *57*, 746–752.
- (46) Aslan, K.; Huang, J.; Wilson, G. M.; Geddes, C. D. Metal-Enhanced Fluorescence-Based RNA Sensing. *J. Am. Chem. Soc.* **2006**, *128*, 4206–4207.
- (47) Abel, B.; Aslan, K. Immobilization of Enzymes to Silver Island Films for Enhanced Enzymatic Activity. *J. Colloid Interface Sci.* **2014**, *415*, 133–42.
- (48) Grell, T. A.; Paredes, E.; Das, S. R.; Aslan, K. Quantitative Comparison of Protein Surface Coverage on Glass Slides and Silver Island Films in Metal-Enhanced Fluorescence-Based Biosensing Applications. *Nano Biomed Eng.* **2010**, *2*, 165–170.
- (49) Abel, B.; Clement, T. C.; Aslan, K. Enhancement of Enzymatic Colorimetric Response by Silver Island Films on High Throughput Screening Microplates. *J. Immunol. Methods* **2014**, *411*, 43–49.

(50) Joseph, R. L.; Lakowicz, R. *Principles of Fluorescence Spectroscopy*; Kluwer Academic/Plenum Publishers: New York, 1999; p 11.

(51) Aslan, K.; Leonenko, Z.; Lakowicz, J. R.; Geddes, C. D. Fast and Slow Deposition of Silver Nanorods on Planar Surfaces: Application to Metal-Enhanced Fluorescence. *J. Phys. Chem. B* **2005**, *109*, 3157–3162.

(52) Aslan, K.; Malyn, S. N.; Zhang, Y.; Geddes, C. D. Conversion of Just-Continuous Metallic Films to Large Particulate Substrates for Metal-Enhanced Fluorescence. *J. Appl. Phys.* **2008**, *103*, 084307-1–084307-7.